Journal of Ceramic Processing Research. Vol. 14, Special. 1, pp. s30~s34 (2013)

J O U R N A L O F
Ceramic Processing Research

Synthesis and luminescence properties of $LiMg_{1-x}Mn_xPO_4$ solid solutions

Xuebin Qiao and Hyo Jin Seo*
Department of Physics, Pukyong National University, Busan 608-737, Republic of Korea

Mn^{2+}-doped $LiMg_{1-x}Mn_xPO_4$ (x = 0.0035-1) solid solutions were prepared by conventional solid state reaction. A systematic structural of the solid solution series was carried out by X-ray powder diffraction. The emission and excitation spectra were employed to characterize the synthesized phosphors. The XRD results reveal that the samples adopt an olivine (Mg_2SiO_4) type structure with the space group Pnma. With increasing Mn^{2+} concentration, the XRD patterns shift systemically to lower angle in indexes of (200), (131), and (211) with all other lines, confirming the formation of solid solutions. The great red-shift of Mn^{2+} emission with increasing Mn^{2+}-concentration from 0.35 to 100 mol% in $LiMg_{1-x}Mn_xPO_4$ is observed. The CIE coordinates and the emission shift of Mn^{2+} ions in $LiMg_{1-x}Mn_xPO_4$ are discussed in relation to the structural properties of $LiMg_{1-x}Mn_xPO_4$.

Key words: Solid solution, Luminescence, Color turning, $LiMg_{1-x}Mn_xPO_4$, Mn^{2+}.

Introduction

An $ABPO_4$ formula is a large family of monophosphates with different types of structure depending on the relative size of the A and B ions, where A is monovalent alkali metal ions and B is divalent alkaline earth metal ions [1]. If the A and B are the smallest ions, i.e. Li^+ and Mg^{2+}, the resulting compound $LiMgPO_4$ adopts the olivine (Mg_2SiO_4) type structure [2]. These kinds of mono-phosphates have attracted much attention because they have interesting magnetoelectric properties [3-6]. The magnetic divalent doping in $ABPO_4$ (A = Li, Rb B = Mg, Co, Ni, Mn) hosts exhibit antiferromagnetic behaviors with some differences in the ordering temperatures [7-9]. The doping of these compounds with magnetic impurities such as Fe introduces a greater complexity not only in the crystal structure but also in the magnetic behavior [10], which means that the Li^+ and Mg^{2+} sites for the impurities play important roles of the behaviors.

Recently, the orthophosphate host family, $A^IB^{II}PO_4$ (A^I: monovalent cation, B^{II}: divalent cation), has been made available as phosphors that combine with near-UV lighting chips for use in solid-state white light-emitting diodes (LEDs) [11-13]. Huang et al [14] reported the unusual luminescence properties ($4f \rightarrow 4f$ transition of Eu^{2+}) of Eu^{2+} ions doped in $LiMgPO_4$. This indicates that the influences of the crystal-field strength and nephelauxetic effect on Eu^{2+} are weak in the $LiMgPO_4$ lattice. Santoro et al [8] reported the magnetic divalent ions replace the magnesium ions in $AMgPO_4$ hosts exhibiting antiferromagnetic behaviors. Hence, it is interesting to investigate luminescence and structural properties of the Mn^{2+} ions doping mechanism in $LiMgPO_4$ host.

Luminescence properties of Mn^{2+}-doped solids, such as oxides, fluorides and sulfides have been intensively investigated during the past decade [15, 16]. The luminescent color of Mn^{2+} varies from green to red depending strongly on the crystal field strength in host lattices [17]. The main band of Mn^{2+} emission is due to the spin forbidden d-d transition of $^4T_1$ (G)-$^6A_1$ (S) with long decay times of a few or several milliseconds. The enhancement of emission intensity and broadening of the excitation peaks can be achieved in solid-solution phosphors, because the sub-lattice structure around the luminescent center ions will be expected to be somewhat diverse, and therefore the spectroscopic lines are expected to be broadened [18]. If two phosphors are isostructural, a solid solution of two phosphors can be formed. Since $LiMgPO_4$ and $LiMnPO_4$ phosphors have the same crystal structure, orthorhombic with a space group of Pnma (No. 62), so it is possible to make solid solution of $LiMg_{1-x}Mn_xPO_4$ (x = 0.0035-1).

In this work, we report solid state syntheses of $LiMg_{1-x}Mn_xPO_4$ (x = 0.0035-1) solid solutions. The luminescence properties are reported for the first time to our knowledge in this host and its relationship with the synthesis condition is discussed. The tunable color emission could be achieved by changing of Mn^{2+} concentration.

Experimental

The preparation of $LiMg_{1-x}Mn_xPO_4$ was carried out by solid state synthesis. The raw materials were Li_2CO_3 (99.9%), $4(MgCO_3)\cdot Mg(OH)_2\cdot 5H_2O$ (magnesium carbonate basic pentahydrate, 99.9%), $NH_4H_2PO_4$ (99.9%) and

*Corresponding author:
Tel : +82-51-629-5568
Fax: +82-51-629-5549
E-mail: hjseo@pknu.ac.kr

$MnCO_3$ (99.9%). The doping level of Mn^{2+} is from 0.35 to 100 mol% of Mg^{2+}. The starting materials with stoichiometric amounts were ground in an agate mortar. The mixture was firstly heated up to 300 °C and kept at this temperature for 5 h. After a second homogenization in the mortar in acetone, the sample was heated up to 500 °C and kept at this temperature for 10 h in air. After that, the sample was mixed and heated at the temperature from 600 to 1000 °C for 10 h in a crucible along with the reducing agent (active carbon). The products were quenched to room temperature.

The crystal structure of the sample was checked by X-ray diffraction (XRD) patterns using a Philips XPert/MPD diffraction system with Cu Ka ($\lambda = 1.5405$ Å) radiation at the room temperature and analyzed using Jade-6.0 software. The luminescence excitation and emission spectra were performed using spectrometer (PTI) equipped with a 150 W Xe lamp at room temperature. The emission spectra with higher resolution were measured under third harmonics (355 nm) of Nd:YAG laser (Spectron Laser Sys. SL802G). The luminescence was dispersed by a 75 cm monochromator (Acton Research Corp. Pro-750) and observed with a photomul-tiplier tube (PMT) (Hamamatsu R928). Suitable filters were used to eliminate the intense laser scattering.

Phase formation and structural analysis

Fig. 1 show the XRD patterns of $LiMg_{0.9}Mn_{0.1}PO_4$ phosphors sintered at different temperature between 600 and 1000 °C. All of diffraction peaks at 900 or 1000 °C are well indexed to $LiMgPO_4$ matching well with JCPDS card of 32-0574. As seen in Fig. 1, no obvious $LiMgPO_4$ phase is found below 800 °C while almost all the diffraction peaks can be indexed to a pure $LiMgPO_4$ at 900 and 1000 °C indicating superior crystallization. However, the phosphor is hard to ground at 1000 °C. It is suggested that the poor crystallinity fired at 600-800 °C was due to the incomplete bonding; however, if temperature reaches higher than 1000 °C, structure of host phosphor was destroyed giving rise to melt. As is well known, the emission and excitation intensity of phosphor is often dependent on the annealing temperature. As will be seen below (inset in Fig. 3), the strongest luminescence intensity could be achieved at 900 °C. Hence, crystalline $LiMg_{0.9}Mn_{0.1}PO_4$ samples were finally formed by heating the milled precursors at 900 °C for 10 h in air atmosphere in a chamber furnace.

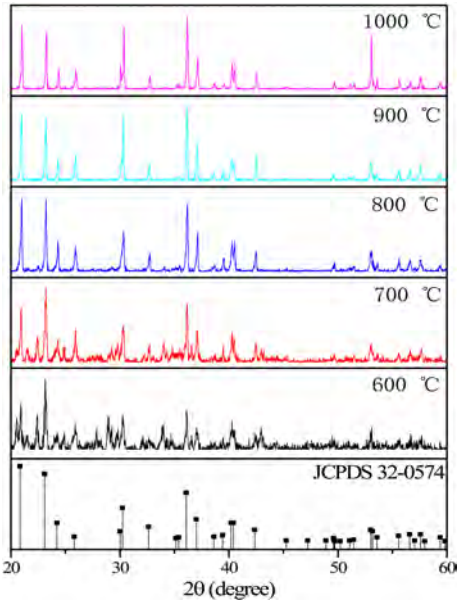

Fig. 1. XRD patterns of phosphor $LiMg_{0.9}Mn_{0.1}PO_4$ precursor annealing at different temperatures for 10 h.

XRD patterns of the $LiMg_{1-x}Mn_xPO_4$ phosphors with x = 0, 0.2, 0.4, 0.6, 0.8 and 1.0 annealed at 900 °C are shown in Fig. 2(a). As in Fig. 2(a), the samples are single phase and all the reflections could be indexed on the basis of the olivine (Mg_2SiO_4) type structure with the space group Pnma [19]. The peak positions of (200), (131), and (211) shift gradually to a lower angle, confirming the formation of solid solutions. For the XRD

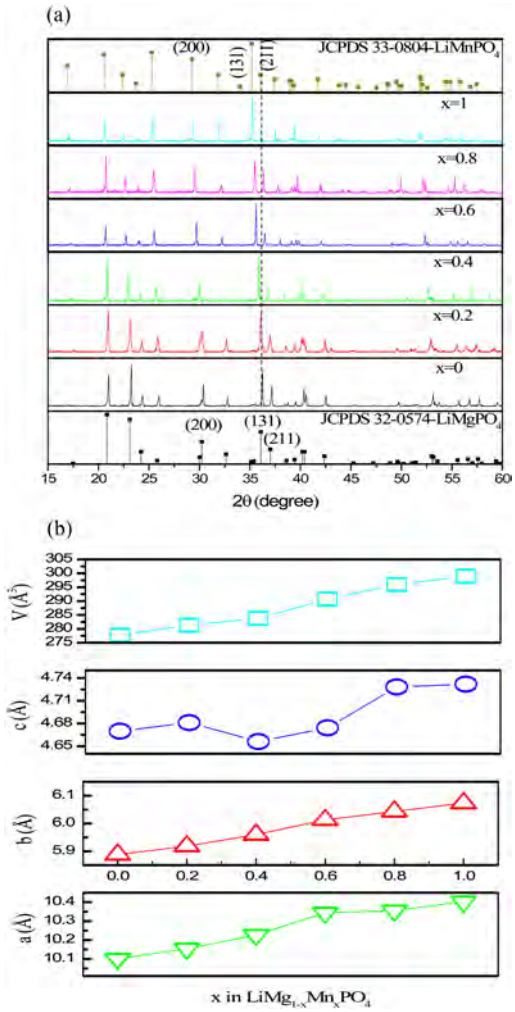

Fig. 2 (a) XRD patterns of the $LiMg_{1-x}Mn_xPO_4$ phosphors which show the continuous shift in the positions of the reflections to low angles with the substitution of bigger Mn^{2+} for Mg^{2+} in $LiMg_{1-x}Mn_xPO_4$ and (b) variations of the unit cell parameters of $LiMg_{1-x}Mn_xPO_4$ with x.

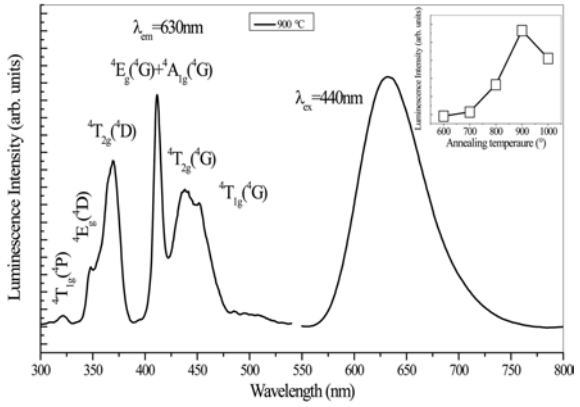

Fig. 3 the excitation spectra and emission spectra of phosphor $LiMg_{0.9}Mn_{0.1}PO_4$ precursor annealing at 900 °C for 10 hours. Inset is the emission intensity as a function of annealing temperatures.

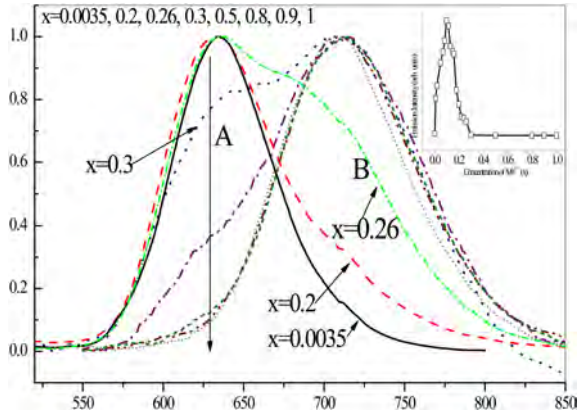

Fig. 4 Normalized Emission spectra with different Mn^{2+} doping concentration in $LiMg_{1-x}Mn_xPO_4$ (x = 0-1) under the excitation of 355 nm at room temperature.

patterns of $LiMg_{1-x}Mn_xPO_4$ phosphors, as x = 0, the pattern matches well with JCPDS card (No. 32-0574) while the pattern is found exactly the same to JCPDS card (No. 33-0804) at x = 1. All the XRD patterns were fitted using Jade 6.0 program by taking the reference of JCPDS cards of 32-0574 and 33-0804. Fig. 2(b) shows the variations of lattice parameters and unit cell volumes as a function of x in $LiMg_{1-x}Mn_xPO_4$. All the unit cell parameters tend to increase by increasing the Mn^{2+} concentration. These plots give a nearly liner relationship indicating the formation of a substitutional solid solution of $LiMg_{1-x}Mn_xPO_4$ (x = 0-1). The systematic variations in lattice parameters and unit cell volume can be understood on the basis of the different ionic radii between the Mn^{2+} ions and its possible substitutional cation in the host. In addition, an analysis of the XRD data by Scherrer's formula revealed an average crystallite size of 50-100 nm for all the solid solutions.

Excitation and emission spectra of $LiMg_{1-x}Mn_xPO_4$

Fig. 3 shows the excitation and emission spectra of $LiMg_{0.9}Mn_{0.1}PO_4$ at room temperature. The excitation spectra consist of several absorption bands associated with Mn^{2+} transition from the ground state $^6A_{1g}(S)$ to the excited states $^4T_{1g}(G)$, $^4T_{2g}(G)$, [$^4A_{1g}(G)$, $^4E_g(G)$], $^4T_{2g}(D)$, $^4E_g(D)$, $^4T_{1g}(P)$ as indicated in the Fig. 3. The spectral features are typical for octahedrally coordinated Mn^{2+} in a host lattice [20]. The most intense excitation peak situated at 410 nm is attributed to the $^6A_{1g}(S) \rightarrow {}^4A_{1g}(G)$, $^4E_g(G)$ transitions; the excitation band at 440 nm can be attributed to the $^6A_{1g}(S) \rightarrow {}^4A_{2g}(G)$ transition, whereas the weak band at 510 nm is ascribed to $^6A_{1g}(S) \rightarrow {}^4A_{1g}(G)$ transition. The emission spectra exhibit broad bands peaking at around 630 nm for all the annealing temperature.

As it is well known, all the optical absorption transitions of Mn^{2+} are parity and spin forbidden. However, this selection rules may be relaxed by the admixture of opposite-parity states due to the crystal field and by lattice vibration [21]. The selection rules are also be relaxed through an exchange mechanism (spin-spin interaction) [22]. In our work, the efficient luminescent emissions of Mn^{2+} were detected. The strong absorption band from 340 to 475 nm in the excitation spectrum indicates that the phosphors can well match with the UV LED chip (360-400 nm) and blue-LED chips (450 nm). Hence, this phosphor is a candidate for phosphors that combine with UV and blue lighting chips for use in solid-state white light-emitting diodes (LEDs).

Concentration dependent emission spectra

The emission spectra of Mn^{2+} are investigated for Mn^{2+} concentration of 0.35-100 mol% in $LiMg_{1-x}Mn_xPO_4$ under the 355 nm excitation at room temperature. The normalized emission spectra for various Mn^{2+} concentrations (0.35-100%) are shown in Fig. 4. With the increasing the Mn^{2+} concentrations, the luminescence intensity increases to a maximum when x = 0.1 and then decreases in the range of x = 0.1-1 shown in the inset in Fig. 4. The asymmetry of the spectra for $LiMg_{1-x}Mn_xPO_4$ (x = 0.0035-1) in Fig. 4 could be reproduced as a superposition of at least two components. Hereafter, the bands at shorter wavelength side and longer wavelength side are called emission band A and B, respectively. As is well known, the Mn^{2+} ion has an emission which consists of a broad band, the position of which depends strongly on the host lattice (crystal field). The influence of the crystal field on the position of the energy levels for the transition metal ion of Mn^{2+} is given by the Tanabe-Sugano diagram for $3d^5$ [23]. The stronger ligand field strength on Mn^{2+} in crystal field, the longer wavelength emission band occurs. So these two emission bands correspond to two different Mn^{2+} sites. Band A could be associated to the Mn^{2+} with weak crystal field while band B is associated to the Mn^{2+} with strong crystal field. Note that when the doping concentration is low ($0.0035 < x \leq 0.2$), only band A is observed while only band B is detected in the heavily doped samples ($0.5 < x \leq 1$). Two bands are

observed when the doping concentration is the region of $0.2 < x \leq 0.5$. It could be found that the relative emission intensity is dependent on the Mn^{2+} doping concentration. When the Mn^{2+} doping concentration (x = 0-0.26) is low, the band A emission is dominant; the band B emission increases in conjunction with a decrease of band A and become dominant until the Mn^{2+} concentration reach to 0.3 or higher.

It is noted that another peak appears at around 711 nm and become dominant with the diminishing of former 630 nm peak as in heavily doped samples. This is to say, the redshift of the Mn^{2+} band emission happens with variation of Mn^{2+} concentration. This Mn^{2+} concentration dependent phenomenon should be understood by taking accounting into the possible substitution sites of Mn^{2+} in the host. $LiMgPO_4$ and $LiMnPO_4$ belong to Pnma (62) space group with Olivine-type. These two isostructural host have slight different dimensions and shapes of polyhedral LiO_6, MgO_6 (MnO_6) and PO_4 in the olivine-type structure. The dimensions of these polyhedral in $LiMnPO_4$ are slightly longer than in $LiMgPO_4$. The main difference between $LiMgPO_4$ and $LiMnPO_4$ is the connection angle of -MgO_6-MgO_6-MgO_6- and -MnO_6-MnO_6-MnO_6- chains. The connection angle of -MgO_6-MgO_6-MgO_6- in $LiMgPO_4$ and -MnO_6-MnO_6-MnO_6- in $LiMnPO_4$ are 101.466 º and 102.433 º. So it is easy to understood the disordered symmetry of Mn^{2+} are expected in $LiMnPO_4$ lattice compared with that in $LiMgPO_4$. Hence the long wavelength emission of Mn^{2+} at 711 nm dominates as it experiences the stronger crystal field strength.

In olivine type $LiMg(Mn)PO_4$ structure, Li is octahedral coordinated by oxygen and Li diffusion from site to site needs to get through adjacent PO_4 tetrahedral sites and $Mg(Mn)O_6$ octahedral sites by hopping [24]. Because Li hops require thermal energy fluctuations, the hopping rate decreases exponentially with energy of activated state, and small reductions in this activation energy can lead to substantial improve-ment of Li diffusion [25]. The energy required for a Li^+ ion to cross the activated state is likely to depend on the size of the LiO_6 octahedra as well as on the cross section area of the lithium ion one-dimension tunnel. Hence, the bigger size of three octahedra, the higher diffusion possibility of Li^+ ion. As mentioned above, the size of LiO_6, PO_4 and MnO_6 octahedra in $LiMnPO_4$ is bigger than that in the $LiMgPO_4$. Consequence, the more disordered structure of octahedral could be expected in $LiMnPO_4$ than that in $LiMgPO_4$ as a result of Li^+ hopping, which gives result of supplying the stronger crystal field for Mn^{2+} ions. Red shift could be expected according to the point mention above.

CIE coordination

Many researches were reported on emission shift of phosphor by controlling the crystal field surrounding the activators in hosts, e.g., Mn^{2+} in ZnS [26], Mn^{2+} in $NaCaPO_4$ [27], Mn^{2+} in $LiZnPO_4$ [28], Mn^{2+} in Zn_2SiO_4 [29] and Eu^{2+} in Ca-α-SiAlON [30]. The color tuning could be achieved by emission shift [31, 32]. The chromaticity diagram established by the Commission Internationale de l'Eclairage (CIE) in 1931 is a two dimensional graphical representation of any color perceivable by the human eye on an x-y plot. To observe the temperature effect on the chromaticity, CIE coordinates were calculated in $LiMg_{1-x}Mn_xPO_4$ (x = 0.0035-1). Fig. 5 shows the chromaticity points of $LiMg_{1-x}Mn_xPO_4$ (x = 0.0035-1). As the concentration of Mn^{2+} is increased, the CIE coordinates (x, y) were varied systematically from x = 0.0035 of (0.6509, 0.3470) to x = 1 of (0.7154, 0.2845). It can be concluded that the amount of Mn^{2+} ions has obvious influence on the position of color point in this diagram. The chromaticity coordinates of $LiMg_{1-x}Mn_xPO_4$ (x = 0.26) are (0.6695, 0.3290). This result is all closer to the standard of National Television Standards Committee (NTSC) (x = 0.67, y = 0.33) than that of commercial red phosphor of $Y_2O_2S:Eu^{3+}$ (0.622, 0.351) [33]. Therefore, the CIE values also indicate red-emitting phosphors $LiMg_{1-x}Mn_xPO_4$ have a potential application in pc-LEDs.

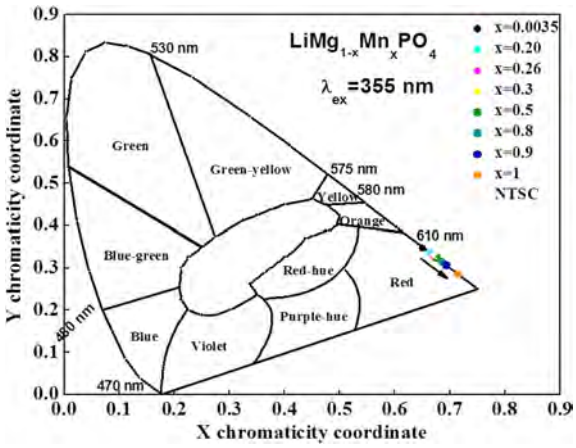

Fig. 5. the CIE chromaticity diagram for $LiMg_{1-x}Mn_xPO_4$ (x = 0.0035-1) phosphors excited at 355 nm. The CIE coordinate of these phosphors with different Mn^{2+} concentration are shown as the colored solid circles. The LT magenta open star is the standard value of NTSC (x = 0.67, y = 0.33).

Conclusions

$LiMg_{1-x}Mn_xPO_4$ (x = 0.0035-1) solid solutions were prepared by conventional solid state reaction. The XRD results reveal that the samples adopt an olivine (Mg_2SiO_4) type structure with the space group Pnma, confirming the formation of solid solutions. By annealing at 900 ºC, the $LiMg_{1-x}Mn_xPO_4$ solid solution gives the optimum luminescence intensity with excellent crystallization. The photoluminescence excitation spectrum shows two broad bands extending from 400 to 475 nm and from 330 nm to 390. All these two bands match well with the blue InGaN LED chip and near UV LED

chip excitation, respectively. Under the excitation of 355 nm, the $LiMg_{1-x}Mn_xPO_4$ solid solution gives a tunable red emission as the variation of concentration of Mn^{2+}. The chromaticity coordinates of $LiMg_{1-x}Mn_xPO_4$ (x = 0.26) are (0.6695, 0.3290) which is very closer to the standard of National Television Standards Committee (NTSC) (x = 0.67, y = 0.33), demonstrating the potential application of single phosphor converted white LEDs.

Acknowledgement

This work was supported by the Mid-career Researcher Program through National Research Foundation of Korea (NRF) grant funded by the Ministry of Education, Science and Technology (MEST) (Project No. 2009-0078682).

References

1. M.B. Amara, M. Vlasse, G. .e Flem, and P. Hagenmuller, Acta Crystallogr. C 39 (1983) 1483-1485.
2. F. Hanic, M. Handlovic, K. Burdova, and J. Majling, J. Cryst. Spectrosc. 12 (1982) 99-127.
3. A.K. Padhi, K.S. Nanjundaswamy, and J.B. Goodenough, J. Electrochem. Soc. 144 (1997) 1188-1194.
4. A. Yamada, M. Hosoya, S.C. Chung, Y. Kudo, K. Hinokuma, K.Y. Liu, and Y. Nishi, J. Power Sources 119 (2003) 232-238.
5. S. Okada, S. Sawa, M. Egashira, J. Yamaki, M. Tabuchi, H. Kageyama, T. Konishi, and A. Yoshino, J. Power Sources 97 (2001) 430-432.
6. J.M. Loris, C. Perez-Vicente, and J.L. Tirado, Electrochem. Solid State Lett. 5 (2002) A234-A237.
7. A. Goñi, L. Lezama, G.E. Barberis, J.L. Pizarro, M.I. Arriortua, and T. Rojo, J. Magn. Magn. Mater. 164 (1996) 251-255.
8. R.P. Santoro, and R.E. Newnham, Acta Crystallogr 22 (1967) 344-347.
9. H. Ben Yahia, E. Gaudin, and J. Darriet, J. Alloys Compd. 442 (2007) 74-76.
10. D. Vaknin, J.L. Zarestky, J.E. Ostenson, B.C. Chacoumakos, A. Goñi, P.J. Pagliuso, T. Rojo, and G.E. Barberis, Phys. Rev. B 60 [2] (1999) 1100-1110.
11. Z.C. Wu, J.X. Shi, J. Wang, M.L. Gong, and Q. Su, J. Solid State Chem. 179 (2006) 2356-2360.
12. P. Dorenbos, L. Pierron, L. Dinca, C.W.E. van Eijk, A.K. Harari, and B. Viana, J. Phys.: Condens. Matter 15 (2003) 511-520.
13. Y.S. Tang, S.F. Hu, C.C. Lin, N.C. Bagkar, and R.S. Liu, Appl. Phys. Lett. 90 (2007) 151108-151111.
14. S.Y. Zhang, Y.L. Huang, L. Shi, and H.J. Seo, J. Phys.: Condens. Matter 22 (2010) 235402-235408.
15. G.G. Li, D.L. Geng, M.M. Shang, C. Peng, Z.Y. Cheng, and J. Lin, J. Mater. Chem. 21 (2011) 13334-13344.
16. J.Y. Zhang, Z.T. Zhang, Z.L. Tang, and Y.H. Lin, Mater. Chem. Phys. 72 (2001) 81-84.
17. G. Blasse, and B.C. Grabmaier, in "Luminescence Materials" (Springer, Berlin Heideberg, 1994) p. 52.
18. Z. Wang, H. Liang, L. Zhou, H. Wu, M. Gong, and Q. Su, Chem. Phys. Lett. 412 (2005) 313-316.
19. F. Hanic, M. Handlovic, K. Burdova, and J. Majling, J. Cryst. Spectrosc. Res. 12 (1982) 99-127.
20. M.C. Marco de Lucas, F. Rodríguez, C. Prieto, M. Verdaguer, and H.U. Güdel, J. Phys. Chem. Solids 56 (1995) 995-1001.
21. G.U. Caldino, J. Phys. Condens. Matter 15 (2003) 7127-7137.
22. B. Henderson, and G.F. Imbusch, in "Optical Spectroscopy of Inorganic Solids" (Oxford University Press, UK 1989) p. 453-494.
23. S. Sugano, Y. Ranabe, and Y.H. Kamimura, in "Multiplets of Transition-Mental Ions in Crystals" (Academic, New York 1970) p. 107.
24. G.K.P. Dathar, D. Sheppard, K.J. Stevenson, and G. Henkelman, Chem. Mater. 23 (2011) 4032-4037.
25. Y.Z. Donga, Y.M. Zhao, and H. Duan, Mater. Chem. Phys. 129 (2011) 756-760.
26. W. Chen, R. Sammynaiken, Y.N. Huang, J. Malm, R. Wallenberg, J. Bovin, V. Zwiller, and N.A. Kotov, J. Appl. Phys. 89 (2001) 1120-1129.
27. S.Y. Zhang, Y.L. Huang, W.F. Kai, L. Shi, and H.J. Seo, Electrochem. Solid-State Lett. 13 [2] (2010) J11-J14.
28. T.S. Chan, R.S. Liu, and I. Baginskiy, Chem. Mater. 20 (2008) 1215-1217.
29. C.R. Ronda, and T. Amrein, J. Lumin. 69 (1996) 245-248.
30. R.J. Xie, N. Hirosaki, K. Sakuma, Y. Yamamoto, and M. Mitomo, Appl. Phys. Lett. 84 (2004) 5404-5406.
31. P.F. Smet, J.E.V. Haecke, F. Loncke, H. Vrielinck, F. Callens, and D. Poelman, Phys. Rev. B. 74 (2006) 035207-035215.
32. V. Bachmann, C. Ronda, O. Oeckler, W. Schnick, and A. Meijerink, Chem. Mater. 21 (2009) 316-325.
33. R. Zhu, Y.L. Huang, and H.J. Seo, J. Electrochem. Soc. 157 (2010) H1116-H1120.